DOI: 10.1002/ejic.201100309

Structural Characterization and Photoluminescent Properties of $(La_{1-x}Sm_x)_2Ti_2O_7$ Solid Solutions Synthesized by a Sol–Gel Route

Zhenmian Shao,[a,b,c] Sébastien Saitzek,*[a,b,c] Jean-François Blach,[a,b,c] Adlane Sayede,[a,b,c] Pascal Roussel,[a,c,d] and Rachel Desfeux[a,b,c]

Keywords: Perovskite phases / Sol–gel processes / Luminescence / Density functional calculations / X-ray diffraction / Raman spectroscopy

A series of compounds with the general formula $(La_{1-x}Sm_x)_2Ti_2O_7$ ($0 \leq x \leq 1.0$) has been synthesized by a sol–gel method and characterized by XRD, Raman spectroscopy, and scanning electron microscopy (SEM). These compounds are structurally isomorphic to perovskite-type $La_2Ti_2O_7$ until a substitution rate of $x = 0.8$. Above this substitution rate ($x > 0.8$), a biphasic mixture is obtained between the substituted perovskite layered phase and the pyrochlore $Sm_2Ti_2O_7$ phase. The unusual phosphor $(La_{1-x}Sm_x)_2Ti_2O_7$ has been elaborated and its luminescent properties were investigated for low rates of substitution. The emission and excitation spectra were used to study the luminescent properties. The $(La_{1.9}Sm_{0.1})_2Ti_2O_7$ powders emit bright red–orange light under UV excitation. The emission properties show that $La_2Ti_2O_7$ is a suitable host where the La^{3+} ions can be substituted by other trivalent lanthanide ions that induce luminescence properties in the visible region and lead to phosphor materials. The electronic structure calculations of $(La_{1.9}Sm_{0.1})_2Ti_2O_7$ shows that this compound is an insulator with a band gap of about 2.77 eV. The valence band mainly consists of oxygen states with hybridized titanium and samarium states; whereas, the conduction band mainly consists of titanium states with hybridized lanthanum and samarium states.

Introduction

Lanthanide titanates of general formula $Ln_2Ti_2O_7$ are the subject of considerable interest due to their photocatalytic and ferroelectric properties. For instance, they can be used as photocatalysts for producing hydrogen from water splitting and degradation of organic pollutants.[1–4] Generally, $Ln_2Ti_2O_7$ compounds (Ln = La, Ce, Pr, Nd) crystallize in a perovskite-layered structure[1,5] and exhibit ferroelectric properties; consequently, they can be used in ferroelectric random access memory[5] and ferroelectric gate field-effect transistors.[6] Moreover, these compounds have a high Curie temperature, which is particularly interesting for high-temperature piezoelectric applications.[7,8] However, Ln^{3+} ions with small radii (Ln = Sm–Lu) generally adopt a pyrochlore structure[9,10] with no known ferroelectric properties. The stability of the structure depends on the ratio between the radii (r) of the Ln^{3+} and Ti^{4+} cation sites. If $r(Ln^{3+})/r(Ti^{4+})$ is in the range 1.46–1.78, then the compound formed will have a pyrochlore structure. However, if $r(Ln^{3+})/r(Ti^{4+})$ is higher than 1.78, then the compound formed will adopt a perovskite-layered structure. If $r(Ln^{3+})/r(Ti^{4+})$ is less than 1.46, the compound will adopt a defect fluorite structure.[9]

$La_2Ti_2O_7$ has been reported to be ferroelectric with a high Curie temperature ($T_c \approx 1500$ °C). It has a dielectric constant in the range $\varepsilon_r = 42–62$, with a low-temperature coefficient and a low dielectric loss at microwave frequency.[11] $La_2Ti_2O_7$ crystallizes in a monoclinic structure with a $P2_1$ space group. The unit cell parameters, number of molecules per unit cell (Z), and theoretical density (ρ) are $a = 7.8114(2)$, $b = 5.5474(1)$, $c = 13.0185(1)$ Å, $\beta = 98.719°$, $Z = 4$, and $\rho = 5.78$ g cm^{-3}, respectively.[12]

$Sm_2Ti_2O_7$ crystallizes in a cubic pyrochlore structure with a $Fd\text{-}3m$ space group. The unit cell parameter, number of molecules per unit cell, and theoretical density are $a = 10.231(1)$ Å, $Z = 8$, and $\rho = 6.305$ g cm^{-3}, respectively.[13,14] Oxides with a pyrochlore structure have been proposed as good candidates for the immobilization of actinide species for nuclear waste.[14,15]

Photoluminescence has been identified in rare earth $Ln_2Ti_2O_7$ doped compounds such as $La_2Ti_2O_7$:Pr^{3+},[16] $Gd_2Ti_2O_7$:Eu^{3+},[17] and $(La_{0.95}Eu_{0.05})_2Ti_2O_7$:$Li^+$.[18] Furthermore, it has been reported that $La_2Ti_2O_7$ oxides can act as excellent hosts for integration by substitution of

[a] Université Lille Nord de France, 59000 Lille, France
[b] Université d'Artois, Unité de Catalyse et de Chimie du Solide, UCCS, Équipe Chimie du Solide, CNRS-UMR 8181, Faculté des Sciences Jean Perrin, 62300 Lens, France
Fax: +33-3-21177955
E-mail: sebastien.saitzek@univ-artois.fr
[c] CNRS, UMR 8181, 59650 Villeneuve d'Ascq, France
[d] USTL, ENSCL, UCCS, 59652 Villeneuve d'Ascq, France

lanthanide ions to produce phosphors emitting a variety of colors for the development of photoluminescent materials.[16,18]

There are several synthesis routes for $Ln_2Ti_2O_7$ compounds (Ln = La and Sm) such as traditional solid-state reactions,[1,19,20] polymerized-complex methods,[21] hydrothermal synthesis,[22] coprecipitation methods,[13] metal–organic decomposition methods,[23] and sol–gel synthesis.[24–26] However, to the best of our knowledge, there is no report of the synthesis of a $(La_{1-x}Sm_x)_2Ti_2O_7$ solid solution.

The objective of this work is to use a sol–gel synthesis method to obtain a $(La_{1-x}Sm_x)_2Ti_2O_7$ solid solution and to study its luminescent properties. Structural characterization was performed by XRD to evidence the evolution of lattice parameters in the as-synthesized solid solution and multiphasic compounds. The morphology and average grain size of the powders were investigated by SEM, and the luminescent properties for the compounds with low rates of substitution were measured. Finally, the electronic structures of the $La_{1.9}Sm_{0.1}Ti_2O_7$ solid solutions, obtained by first principle calculations, were analyzed to give a better understanding of their optical properties.

Results and Discussion

Structural Characterization and Morphology

XRD patterns of $Sm_2Ti_2O_7$ powders prepared by the sol–gel route under different temperatures are shown in Figure 1 within the 2θ range of 10° to 90°. This step was undertaken to determine the optimum synthetic temperature of undoped $Sm_2Ti_2O_7$. We observe that $Sm_2Ti_2O_7$ (JCPDS No. 15–0209) crystallizes in cubic pyrochlore structure and begins to form at 800 °C. The XRD peak intensity increases slowly with temperature until 1100 °C. The full width at half maximum value of the peaks decreases as the temperature increases. Similar results for the preparation of $La_2Ti_2O_7$ layered-perovskite structures were obtained in previous work.[27] We chose a temperature of 1100 °C for the calcination of the $(La_{1-x}Sm_x)_2Ti_2O_7$ gels (x = 0–1) to obtain good crystallinity.

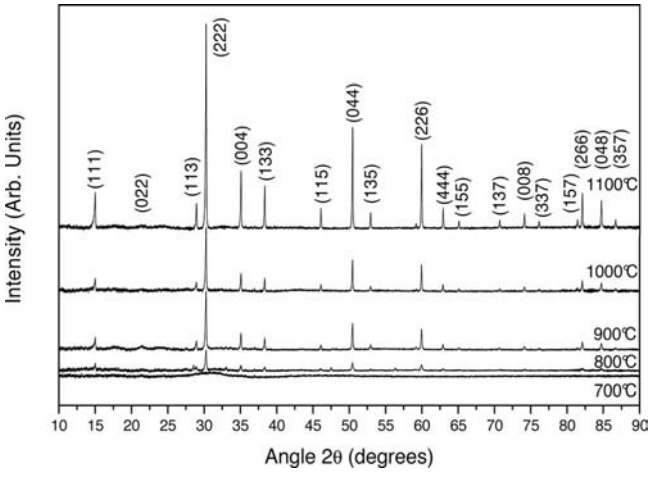

Figure 1. XRD patterns of $Sm_2Ti_2O_7$ obtained at various calcination temperatures.

XRD patterns of $(La_{1-x}Sm_x)_2Ti_2O_7$ (x = 0–1) are shown in Figure 2. For x = 0–0.8, we observe the perovskite-type structure of $La_2Ti_2O_7$ (JCPDS No. 81–1066), without ad-

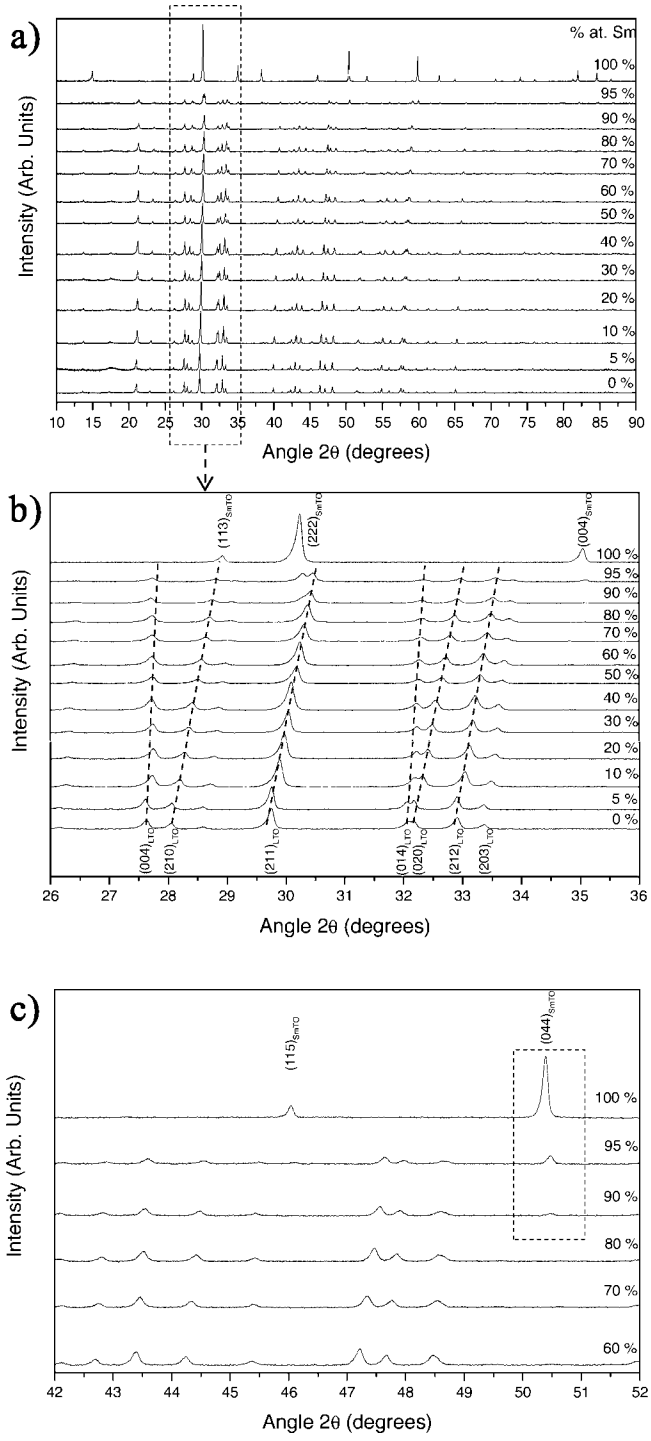

Figure 2. (a) XRD patterns of $(La_{1-x}Sm_x)_2Ti_2O_7$ powders for various atomic percentage of Sm; (b) the (hkl) peak positions (with h and $k \neq 0$) changes depending on x values, whereas the (00l) peak position remains unaffected; (c) the presence of $Sm_2Ti_2O_7$ pyrochlore phase is observed for atomic percentages above 80% (see dotted part).

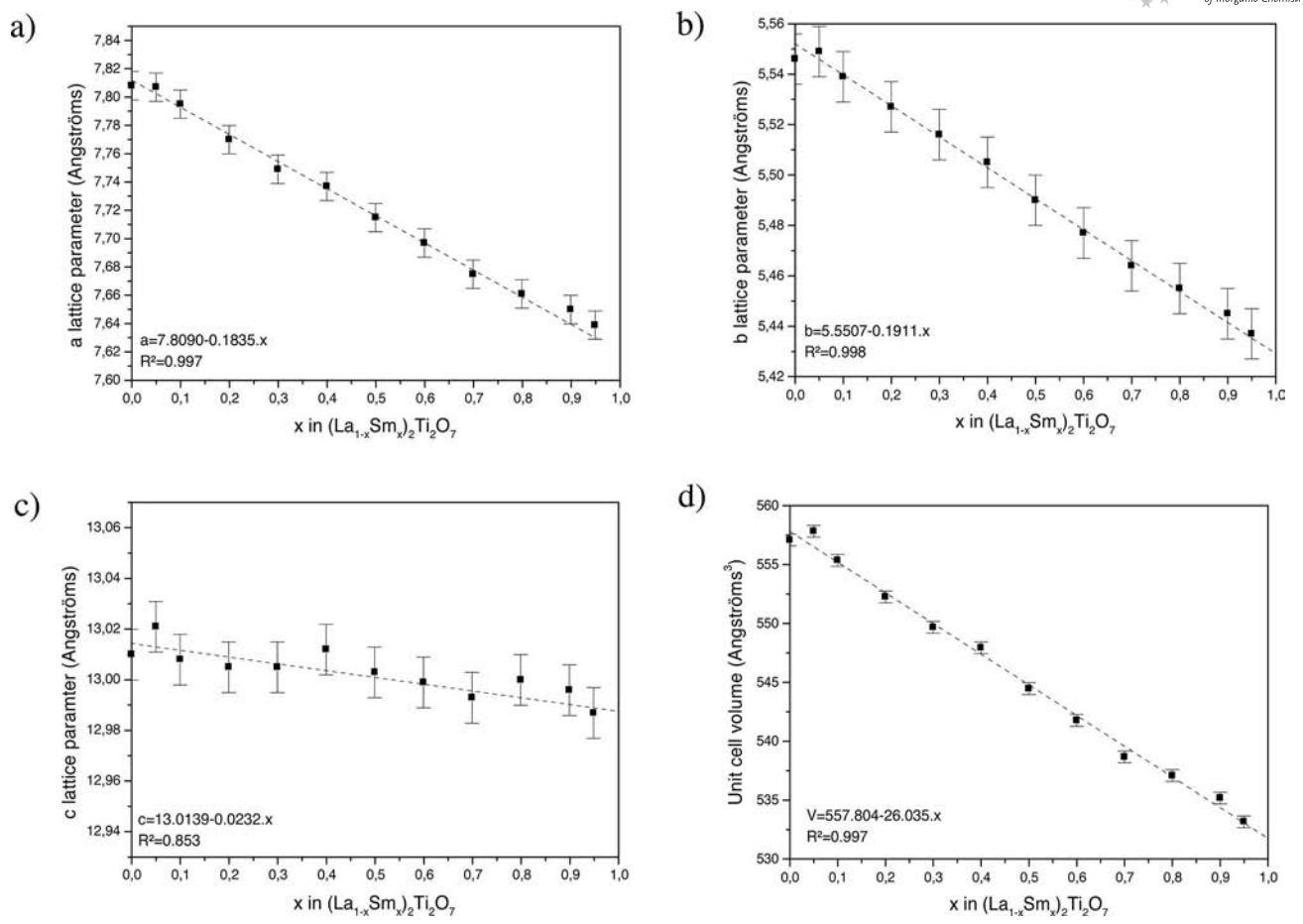

Figure 3. Evolution of $(La_{1-x}Sm_x)_2Ti_2O_7$ unit cell parameters vs. x.

Table 1. Unit cell parameters of $(La_{1-x}Sm_x)_2Ti_2O_7$ powders calculated using the Unit Cell program based on the refinement of 2θ observed with the (hkl) theoretical values of $La_2Ti_2O_7$ (JCPDS No. 81–1066). The star indicates that $Sm_2Ti_2O_7$ was refined using pyrochlore structure (JCPDS No. 15–0209).

% at. Sm	a (Å)	b (Å)	c (Å)	β (°)	V (Å^3)
0	7.808(4)	5.546(4)	13.010(1)	98.646(5)	557.08(5)
5	7.807(8)	5.549(3)	13.021(8)	98.633(4)	557.82(2)
10	7.795(0)	5.539(7)	13.008(2)	98.637(3)	555.35(6)
20	7.770(8)	5.527(6)	13.005(1)	98.661(6)	552.26(0)
30	7.749(0)	5.516(9)	13.005(2)	98.643(6)	549.67(0)
40	7.737(3)	5.505(6)	13.012(0)	98.690(9)	547.93(8)
50	7.715(4)	5.490(2)	13.003(0)	98.691(8)	544.47(6)
60	7.697(3)	5.477(5)	12.999(5)	98.712(8)	541.77(3)
70	7.675(0)	5.464(5)	12.993(7)	98.715(7)	538.67(5)
80	7.661(3)	5.455(8)	13.000(3)	98.733(8)	537.09(4)
90	7.650(6)	5.445(9)	12.996(4)	98.759(4)	535.18(3)
95	7.639(6)	5.437(1)	12.987(7)	98.771(9)	533.17(5)
100*	10.233(1)	–	–	90	1071.57(2)

ditional peaks. These compounds have a monoclinic structure with $P2_1$ space group. The intermediate compositions ($0 \leq x \leq 0.8$) have the same structural type. The refined lattice parameters are shown in Table 1. Firstly, parameters a and b decrease with the increase of x: 7.80 to 7.63 and 5.54 to 5.43 Å, respectively. Secondly, c seems quasiconstant for all values of x (13.01 to 12.98 Å). This is directly illustrated by zooming into the XRD pattern in the range of 2θ = 26–36° (Figure 2b). Indeed, we can observe that the (hkl) peaks (with h and $k \neq 0$) move with increasing x value while the (00l) peak positions remain unchanged. Thus, reducing a and b induces a decrease in the cell volume. By plotting the variation of these lattice parameters vs. the x values (Figure 3), we can see that they follow Vegard's law.[28] This linear variation confirms the formation of a solid solution with Sm^{3+} ions inserted in the place of La^{3+} ions without changing the original monoclinic perovskite-type structure. The variation of a and b can be explained by the structure of $La_2Ti_2O_7$; the crystalline structure can be described as layers of distorted perovskite-like slabs corresponding to four corner-sharing TiO_6 octahedra separated by two layers of Ln cation sites (Figure 4). Following the $\vec{a}$ and $\vec{b}$ axes, these compoundspresent infinite chains of TiO_6 octahedra. However, following the $\vec{c}$ axis, we see repetitions of four blocks of TiO_6 octahedra (perovskite n = 4). Variation of the cation size (La^{3+} = 1.160, Sm^{3+} = 1.079 Å)[29] in the perovskite cage significantly changes the values of a and b because the infinite chains are connected in the direction of

these two parameters. On the contrary, following the $\vec{c}$ axis, the TiO_6 octahedra are only connected by four blocks. Thus, modification of the cation size does not significantly affect the value of *c*.

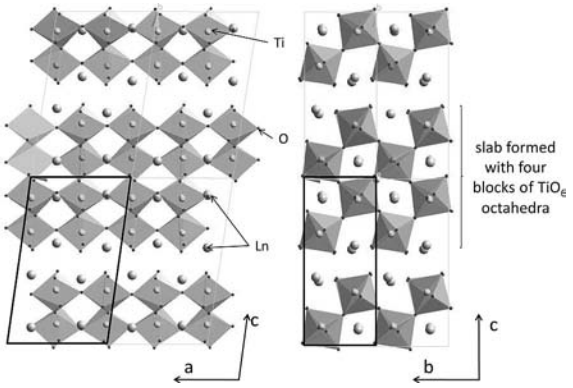

Figure 4. Crystal structure of $Ln_2Ti_2O_7$ (monoclinic $P2_1$). The unit cell is outlined.

For *x* above 0.8, we observe a biphasic mixture consisting of the $Sm_2Ti_2O_7$ cubic pyrochlore structure and the $(La_{1-x}Sm_x)_2Ti_2O_7$ monoclinic layered-perovskite structure. The appearance of the $Sm_2Ti_2O_7$ phase is observed in Figure 2c. Nevertheless, we still observe lattice parameter evolution for the perovskite-layer structure until $x = 0.95$. Finally for $x = 1$, the well known single $Sm_2Ti_2O_7$ cubic pyrochlore phase is seen without additional peaks.

Figure 5 shows SEM images for powders with $x = 0$, 0.1, 0.5, and 1. No significant change in grain shape is observed except for $x = 1$, where the grain shape is more spherical. The average size was determined by a statistical study. The average size and dispersion are 0.70 ± 0.15, 0.20 ± 0.10, 0.40 ± 0.10, and 0.50 ± 0.15 μm for $x = 0$, 0.1, 0.5, and 1, respectively. The La/Sm ratio was verified in all samples by energy dispersive spectroscopy. Moreover, no heterogeneity in the chemical analysis was evidenced.

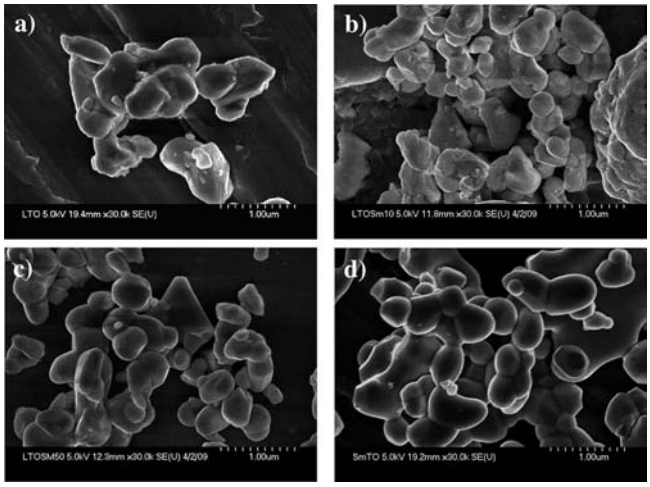

Figure 5. Typical SEM images of $(La_{1-x}Sm_x)_2Ti_2O_7$ powders: (a) $La_2Ti_2O_7$, (b) $La_{1.8}Sm_{0.2}Ti_2O_7$, (c) $LaSmTi_2O_7$, (d) $Sm_2Ti_2O_7$.

Raman Spectroscopy

Raman spectra were initially recorded in the 40–1000 cm^{-1} range (Figure 6a). Firstly, we can observe that the spectrum of $Sm_2Ti_2O_7$ ($x = 1$) is different to the other spectra, but can be assigned by the Raman bands of the pyrochlore $Sm_2Ti_2O_7$.[30] Secondly, we noticed that the other Raman spectra have similar characteristics with some band shifts. The Raman spectrum of pure $La_2Ti_2O_7$ was compared to that in the literature and we found good agreement with the spectrum of the layered perovskite $La_2Ti_2O_7$ obtained by Krishnankutty et al (Table 2).[31] The $La_2Ti_2O_7$ signature is observed for all samples of the solid solutions ($x = 0$–0.95), although the presence of the pyrochlore phase (starred in Figure 6a) is observed in the Raman spectrum of the sample with $x = 0.95$, with the A_{1g} and $E_g + F_{2g}$ bands of $Sm_2Ti_2O_7$ at 513 and 307 cm^{-1}, respectively. These results confirm the behavior observed by XRD. Moreover, we noticed the splitting of the large twin band situated at around 808 cm^{-1}. This splitting appears above $x = 0.4$ and indicates the introduction of Sm atoms and, consequently, the change in lattice parameters.

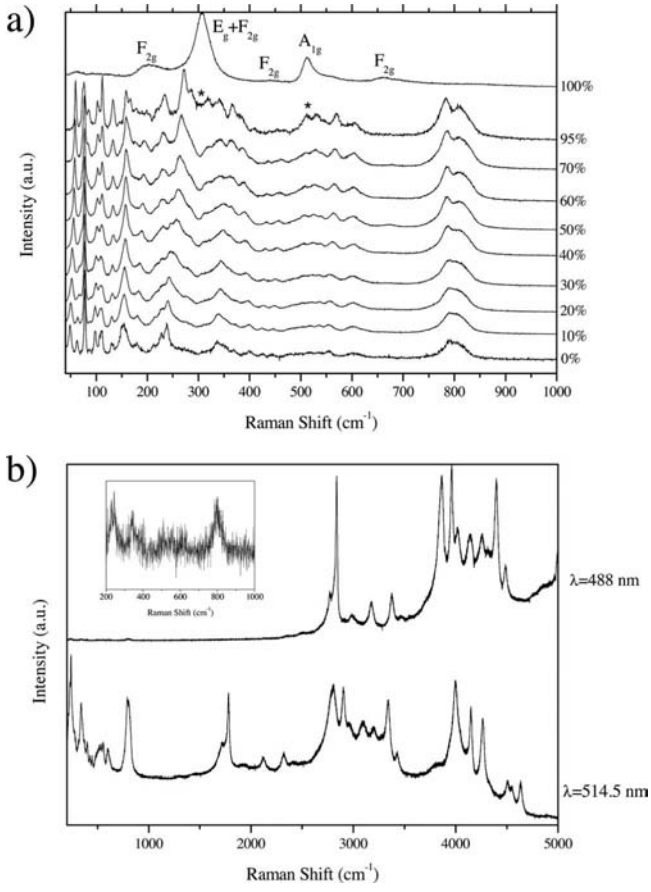

Figure 6. (a) Raman spectra of $(La_{1-x}Sm_x)_2Ti_2O_7$ powders for different atomic percentages of Sm (stars represent the pyrochlore phase); (b) Raman spectra of $(La_{0.9}Sm_{0.1})_2Ti_2O_7$ powders obtained with two excitation laser lines: 488 and 514.5 nm. Inset is shown a closer look at the Raman spectrum obtained in the range 200–1000 cm^{-1} with the 488 nm line.

Table 2. Possible assignment for Raman bands of $La_2Ti_2O_7$ layered perovskite.

Raman Band (cm^{-1})	Assignment
820, m	B_{2g} (TiO_2) 826 cm^{-1}
790, m	
605, w	A_{1g} (TiO_2) 612 cm^{-1}
554, w	La–O
445, vw	E_g (TiO_2) 447 cm^{-1}
343, m	La–O
240, m	La–O
153	La–O
130	B_{1g} (TiO_2) 143 cm^{-1}
110	
97	
78	
63	
49	

We also performed the acquisition of a large Raman spectrum of $(La_{0.9}Sm_{0.1})_2Ti_2O_7$ using 514.5 nm excitation, and we found unexpected bands in the 1500–5000 cm^{-1} region (Figure 6b). These bands cannot be assigned to Raman lines and are attributed to photoluminescent emission lines. To verify this hypothesis we measured a second Raman spectrum of this sample using another excitation line (λ = 488 nm). We noticed the presence of the previous bands but with a global shift corresponding exactly to the difference of the two excitation wavelengths, leading to the conclusion that these bands are due to photoluminescent phenomena.

Electronic Structure of $La_{1.9}Sm_{0.1}Ti_2O_7$

The total density of states (DOS) and the La, Sm, Ti, and O contributions (projected within their atomic spheres) for $La_{1.9}Sm_{0.1}Ti_2O_7$ are depicted in Figure 7 using the GGA+U approach. It is found that the spin-majority DOS in the valence band region from –4.42 to 0 are predominated by O 2p orbitals, which are hybridized with the Ti 3d orbitals from –3.60 to –1.40 eV and with the Sm 4f orbitals from –4.20 to –3.10 eV. This indicates the presence of a covalent contribution to the Ti–O and Sm–O bonding. The spin-minority DOS in the valence band region from –4.17 to 0 eV are predominated by O 2p orbitals, which are hybridized with the Ti 3d orbitals from –3.98 to –1.42 eV. Conversely, the states in the conduction band region from 2.77 to 4.46 eV have a dominant contribution from the Ti 3d orbitals, which are hybridized with the O 2p orbitals and Sm 4f orbitals to a small extent (for the spin-majority DOS). Above 4.78 eV, the conduction band states are composed of Ti 3d, La 4f, La 5d, Sm 4f, and Sm 5d orbitals

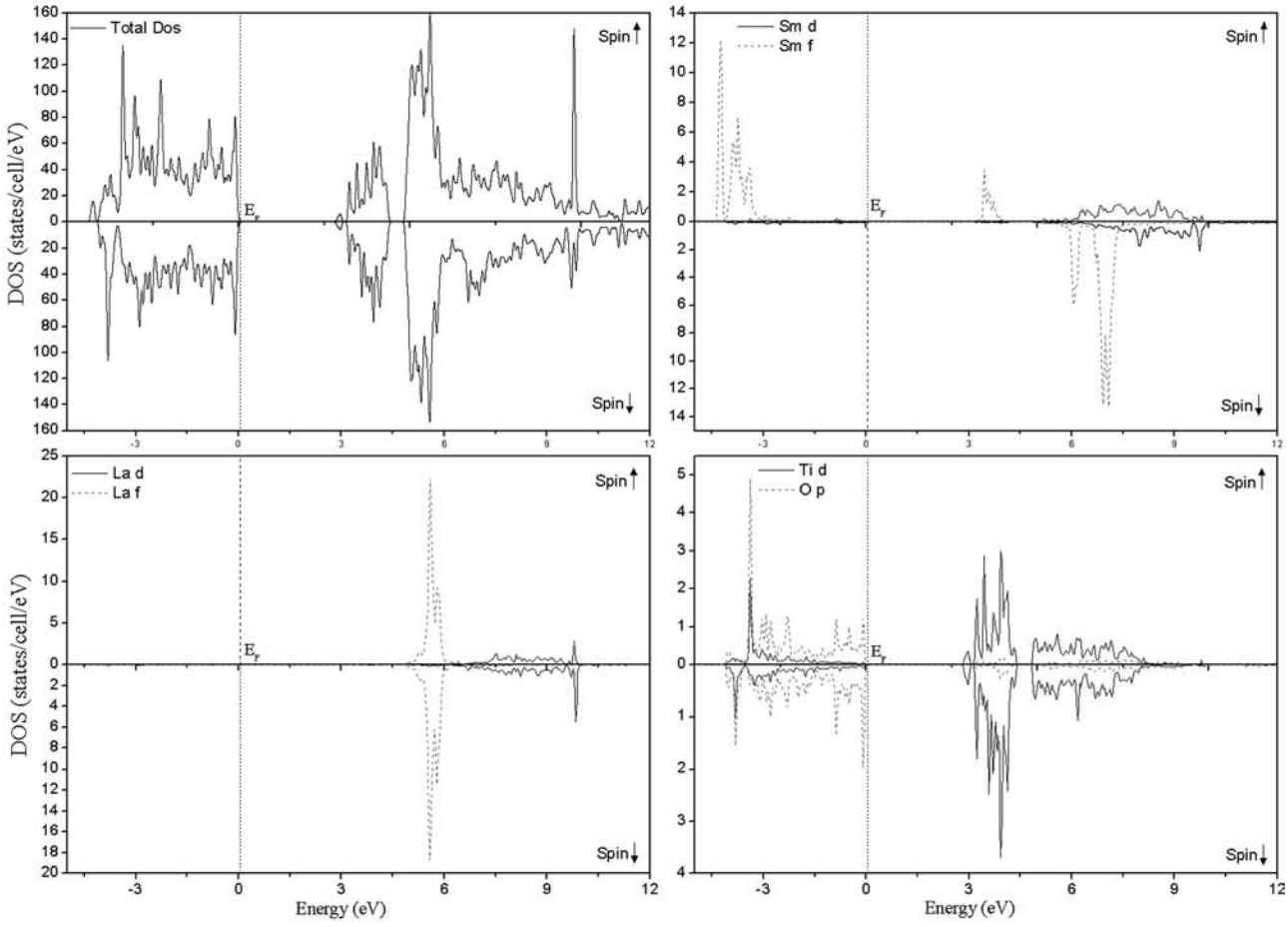

Figure 7. Total DOS, La, Sm, Ti, and O contributions (projected inside their atomic spheres) to the DOS using GGA+U. Lower lying states below –5 eV (not shown) originate from O 2s, La 5p, and Sm 5p orbitals. The Fermi energy is set at zero.

which are hybridized to a small extent with the O 2p orbitals. The presence of sharp peaks around 5.60 eV indicates the localized character of the La 4f states.

The conduction bands are separated from the valence bands by a band gap of 2.77 eV. It should be pointed out that DFT calculated band gaps are smaller than the experimental values. This discrepancy is due to the discontinuity of the exchange–correlation potential, which cannot be taken into account within the Kohn–Sham scheme.[32] For instance, the DFT calculated band gap of $La_2Ti_2O_7$ is about 2.84 eV,[33] whereas experimental band gaps vary from 3.29 to 3.82 eV.[1,34,35]

Luminescent Properties

The $La_2Ti_2O_7$ sample (Figure 8a), presents emission peaks at 608 and 468 nm at room temperature (λ_{ex} = 292 nm), and the broad peak at 760 nm is due to the sample holder. $La_2Ti_2O_7$ is reported to have a direct band gap indicating its potential as a photocatalyst.[34] Logically, La^{3+} does not exhibit luminescence because it has no 4f electrons and there are no energy levels permitting it to induce a luminescent process in the visible region (the La^{3+} ion has a [Xe]$4f^0$ inert gas configuration leading to a $^1S_0$ ground state). Excited states can arise from a p–d transition corresponding to the electronic configuration $5s^25p^55d^1$ which gives rise to the singlet $^1P_1$, $^1D_2$, and $^1F_3$ and triplet $^3P_1$, $^3D_2$, and $^3F_3$ states.[36] Joseph et al.[37] also observed an emission peak near 611 nm, which was explained by the stimulated emission (SE) of transition metal activator Ti^{3+} ions. Electronic transitions of La^{3+} ions enhance this SE (sharp due to the presence of the 4f orbital). In Figure 8b, we can observe the $La_2Ti_2O_7$ white powder under natural light has a reddish color under UV light (254 nm).

For the room temperature emission spectra of the $(La_{1-x}Sm_x)_2Ti_2O_7$ powders obtained with an excitation at 292 nm, we observe an emission peak for $(La_{1-x}Sm_x)_2Ti_2O_7$ with $0.00 \leq x < 0.20$ (see the spectrum obtained for $La_{1.9}Sm_{0.1}Ti_2O_7$ in Figure 8c) in the red spectral area (550 to 710 nm). For the higher x values, these intense peaks vanish. According to the Dieke diagram,[38] Sm^{3+} can present several excitation bands in this wavelength range. Several excitation bands are identified and assigned to the electronic transitions of $^6H_{5/2} \rightarrow {}^4L_{17/2}$ at 363, $^6H_{5/2} \rightarrow {}^6P_{5/2}$ at 376, $^6H_{5/2} \rightarrow {}^4F_{7/2}$ at 403, $^6H_{5/2} \rightarrow {}^4P_{5/2}$ at 420, $^6H_{5/2} \rightarrow {}^4G_{9/2}$ at 440, and $^6H_{5/2} \rightarrow {}^4I_{13/2}$, $^4I_{11/2}$, $^4I_{9/2}$ at 463, 472, and 482 nm, respectively.[39] The excitation spectrum (by monitoring the emission peak at 608 nm) exhibited an intense broad peak at ca. 292 nm due to the $La_2Ti_2O_7$ (or $La_{1.9}Sm_{0.1}Ti_2O_7$) host lattice adsorption. We also observe a less intense peak at 340 nm (3.65 eV), which can be attributed to the charge transfer transition between $O^{2-} \rightarrow Sm^{3+}$.[39,40] There is a good correlation between these experimental values and the DOS calculations presented above.

The emission spectrum exhibited a bright orange–red emission under a UV source, which corresponds to transitions from the excited $^4G_{5/2}$ to the lower levels ^6H_J (J = 5/2, 7/2, 9/2, 11/2) levels of the $4f^5$ configuration of Sm^{3+}[41]

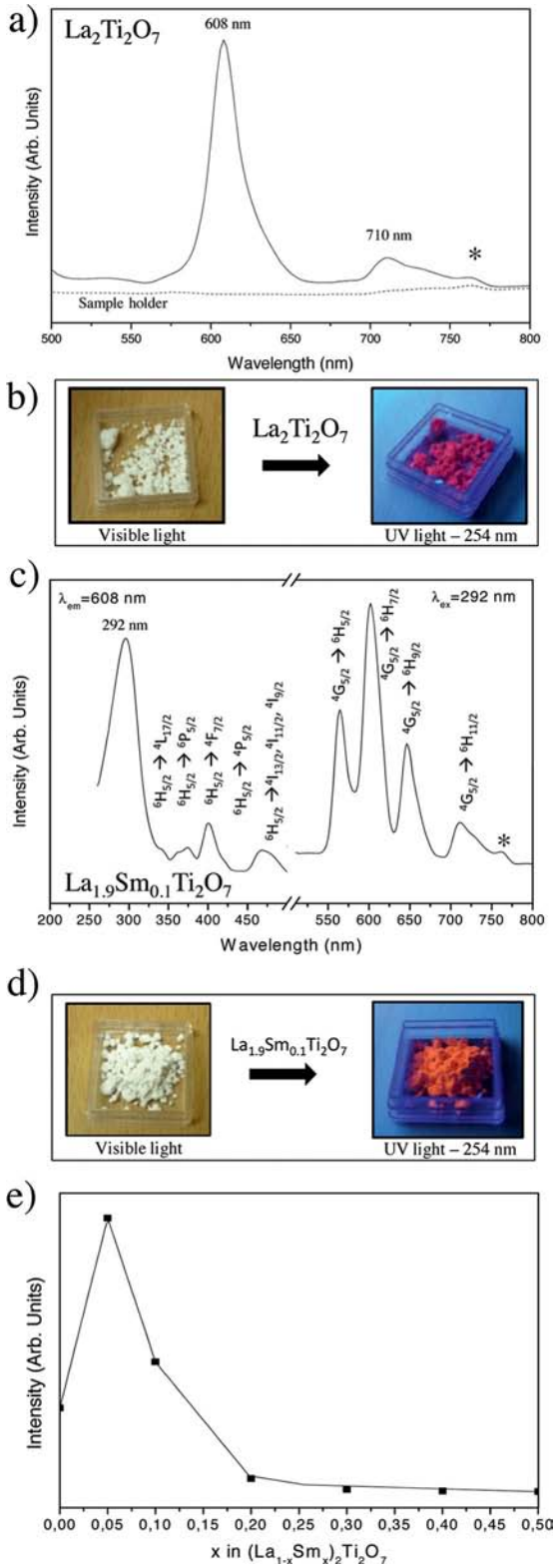

Figure 8. (a) Emission spectrum of pure $La_2Ti_2O_7$ for λ_{ex} = 292 nm (the dotted line represents the emission spectrum of the sample holder and the starred peak due to sample holder); (b) photographs of $La_2Ti_2O_7$ compound under natural light and UV light; (c) excitation and emission spectra of the $La_{1.9}Sm_{0.1}Ti_2O_7$; (d) photographs of $La_{1.9}Sm_{0.1}Ti_2O_7$ compound under natural light and UV light; (e) dependences of the luminescence intensity of $(La_{1-x}Sm_x)_2Ti_2O_7$ solid solutions according to x atomic fraction for the emission peak centred at 565 nm.

located at 565, 605, 647, and 710 nm, respectively. Under UV excitation, a nonradiative transition occurs between the higher energy states to $^4G_{5/2}$ state.[42] The peak located at 710 nm, assigned to the $^4G_{5/2} \rightarrow {}^6H_{11/2}$ transition, has an asymmetric shape, which could consist of two overlapping bands: one at 710 nm due to the transition described above and the other, near 735 nm, could be due to the presence of Sm^{2+}.[43,44] Finally, Figure 8d shows a photograph of $La_{1.9}Sm_{0.1}Ti_2O_7$ under natural and UV light. We clearly observe the effect of luminescence with an emission in the orange region.

We also observe a dependence of the emission intensity on the Sm^{3+} ion concentration (Figure 8e). The emission is maximized at $x = 0.05$ and decreases quickly when the Sm^{3+} concentration exceeds $x = 0.05$ due to concentration quenching. However, the intensity could be even more important for lower substitution rates (less than 0.05 at.%). A study of the luminescent properties vs. x (x = 0–0.5) is therefore essential and will be the subject of our next investigation. Concentration quenching is frequently observed in lanthanide-based phosphors when the substitution level increases.[45,46] It is often ascribed to a nonradiative energy transfer from one activator to another, the probability of which increases with increasing activator concentration.[47] Blasse[48,49] indicated that the nonradiative energy transfer can be expressed by the critical transfer distance (R_c), which represents the distance between the activators to the quenching concentration noted x_c. R_c is calculated by the following equation:

$$R_c = 2\left(\frac{3V}{4\pi x_c N}\right)^{1/3}$$

where V is the unit cell volume (from Table 1) and N is the number of ions whose sites are partially occupied by the activator in the unit cell (in this case $N = 4$). For $x_c = 0.5$, the critical transfer distance is about 8.1 Å. This value should be taken with caution and might be underestimated. To determine a more accurate value, a study in concentration between 0 and 0.5 must be carried out.

$La_2Ti_2O_7$ contains four crystallographic sites available for the activator (substitutes for La^{3+}). Two are among the octahedra and the other two in the planes between the slabs. Generally, $^4G_{5/2} \rightarrow {}^6H_{7/2}$ is a symmetry-sensitive transition emission and $^4G_{5/2} \rightarrow {}^6H_{9/2}$ is an electric-dipole transition. The latter should be forbidden for Sm^{3+} in a symmetric site.[50] We observe the presence of these two emission bands and can therefore conclude that the Sm^{3+} ions are positioned randomly on the crystallographic sites in the $La_2Ti_2O_7$ host lattice.

Conclusions

$(La_{1-x}Sm_x)_2Ti_2O_7$ solid solutions with layered-perovskite structure have been successfully synthesized by a sol–gel method until $x \leq 0.8$ as studied by XRD. The compounds are isomorphous to $La_2Ti_2O_7$ with monoclinic symmetry ($P2_1$ space group). This isomorphism suggests that these compounds have ferroelectric properties like the family of layered perovskites such as $La_2Ti_2O_7$, $Ce_2Ti_2O_7$, $Pr_2Ti_2O_7$, and $Nd_2Ti_2O_7$. Above $x = 0.80$, a biphasic mixture is obtained between the substituted $(La_{1-x}Sm_x)_2Ti_2O_7$ phase and the pyrochlore $Sm_2Ti_2O_7$ phase (*Fd*-3*m* space group). SEM analysis shows that the powders are homogeneous in shape. Raman spectroscopy shows, for low substitutions, luminescent properties induced by Sm^{3+} ions. The analysis performed by spectrofluorometry allowed us to assign the various transitions observed. Emission spectra indicated that $La_{1.9}Sm_{0.1}Ti_2O_7$ materials could be useful for developing new colored light sources, photoluminescent display devices, UV sensors, and conversion phosphors for white-light LEDs.

Experimental Section

$(La_{1-x}Sm_x)_2Ti_2O_7$ powders with various x values were synthesized using a sol–gel method. This method of synthesis has been described in detail for the elaboration of $(La_{1-x}Nd_x)_2Ti_2O_7$ solid solution in previous work.[27] Lanthanum nitrate [$La(NO_3)_3{,}6H_2O$, 99.99%, Sigma Aldrich], samarium nitrate [$Sm(NO_3)_3{,}6H_2O$, 99.9%, Alfa Aesar], and titanium isopropoxide [$Ti\{OCH(CH_3)_2\}_4$, 98.0%, Acros Organics] were used as starting materials. First, a solution of 2,4-pentadione ($CH_3COCH_2COCH_3$, 99+%, Sigma Aldrich) was mixed in a 2-methoxyethanol [$HO(CH_2)_2OCH_3$, 99.0%, Sigma Aldrich] at ambient temperature with stirring for two hours. Then, the titanium isopropoxide [$Ti(OiPr)_4$] was added and the mixture was stirred for two hours. Separately, the stoichiometric lanthanum nitrate and/or samarium nitrate were dissolved in a 2-methoxyethanol solution at approximately 40 °C. The molar ratio [La and/or Sm precursors/$Ti(OiPr)_4$/2,4-pentadione/2-methoxyethanol] was 1:1:1.5:25.5. Finally, the solution containing titanium was added to the lanthanum–samarium solution with continuous stirring at approximately 40 °C over three hours. The gels obtained were dried at 100 to 300 °C for three hours, and then calcined at 700 °C for six hours. The powders were ground and heated from 700 to 1100 °C for twelve hours.

Structural characterizations were carried out by XRD. The XRD patterns for the powders were recorded from 2θ = 10–90° with a Bruker D8 diffractometer in a Bragg–Brentano Setup, equipped with copper X-ray source ($\lambda\bar{K}_\alpha$ = 1.5418 Å). Lattice parameters were refined using the Unit Cell program based on refining 2θ observed with the (*hkl*) theoretical values of $La_2Ti_2O_7$ (JCPDS No. 81–1066). Grain morphologies and average grain sizes were observed by SEM (SEM FEG Hitachi 5–4700). Luminescent properties were studied by the Raman spectroscopy and by photoluminescence spectroscopy. Raman spectra were recorded in back scattering geometry using a Dilor XY800 triple monochromator spectrometer coupled with a microscope which focused the 514.5 nm Ar^+Kr^+ laser beam to a 2 μm spot. The spectra were recorded in the range of 40–1000 cm^{-1}. Luminescence measurements on the spectral range 200–900 nm were performed using a SAFAS Xenius XOF spectrometer.

The electronic structures for $La_{1.9}Sm_{0.1}Ti_2O_7$ were calculated using the WIEN2K package.[51] This DFT-based software implements the augmented plane wave plus local orbitals (APW)+lo method. The plane-wave cutoff, defined by the product of the smallest atomic sphere radius times the magnitude of the largest reciprocal-lattice vector (RMTmin. Kmax), was set to 7.0 and a Gmax (magnitude of the largest vector in the charge-density Fourier expan-

sion) of 12 was used for all calculations. The muffin-tin radius (RMT) of the different atoms are: RMT(La) = 2.30, RMT(Sm) = 2.35, RMT(Ti) = 1.80, and RMT(O) = 1.60 a.u. As it is well known that GGA fails to predict the correct electronic ground states of systems with strongly correlated electrons, we have calculated the electronic structure within the GGA+U method.[52] In this framework, the strong Coulomb repulsion between localized f states is treated by adding a Hubbard-like term to the effective potential, leading to an improved description of correlation effects. As there is no unique way of including a Hubbard term within the DFT framework, several different approaches exist, which all give similar results. In this work we used the approach described by Dudarev et al.[53] where only an effective Hubbard parameter $U_{eff} = U - J$ enters the Hamiltonian. The U_{eff} value is taken to be 6.5 eV. The $La_{1.9}Sm_{0.1}Ti_2O_7$ solid solution is defined by a $2 \times 2 \times 1$ $La_2Ti_2O_7$ supercell where one La atom is substituted by a Sm atom. The numerical integration of the Brillouin zone was performed using a discrete $1 \times 1 \times 4$ Monkhorst–Pack k point sampling.

Acknowledgments

The authors gratefully acknowledge the Nord-Pas de Calais Region and the Centre National de la Recherche Scientifique (CNRS) for financial support of this work. Specifically, this study was conducted as part of a MaProSu project. We also thank Nora Djelal for her help with scanning electron microscopy.

[1] M. Uno, A. Kosuga, M. Okui, K. Horisaka, S. Yamanaka, *J. Alloys Compd.* **2005**, *400*, 270.
[2] R. M. Navarro, F. del Valle, J. A. Villoria de la Mano, M. C. Álvarez-Galván, J. L. G. Fierro, *Adv. Chem. Eng.* **2009**, *36*, 111.
[3] Z. Li, H. Xue, X. Wang, X. Fu, *J. Mol. Catal. A* **2006**, *260*, 56.
[4] D. W. Hwang, H. G. Kim, J. Kim, K. Y. Cha, Y. G. Kim, J. S. Lee, *J. Catal.* **2000**, *193*, 40.
[5] W. S. Kim, S. M. Ha, S. Yun, H. H. Park, *Thin Solid Films* **2002**, *420–421*, 575.
[6] W. S. Kim, S. M. Ha, J. K. Yang, H. H. Park, *Thin Solid Films* **2001**, *398–399*, 663.
[7] J. K. Yamamoto, A. S. Bhalla, *J. Appl. Phys.* **1991**, *70*, 4469.
[8] M. Kimura, S. Nanamatsu, T. Kawamura, S. Matsushita, *Jpn. J. Appl. Phys.* **1974**, *13*, 1473.
[9] M. A. Subramanian, G. Aravamundan, G. V. Subbas Rao, *Prog. Solid State Chem.* **1983**, *15*, 55.
[10] A. V. Shlyakhtina, A. V. Knotko, M. V. Boguslavskii, S. Yu. Stefanovich, D. V. Peryshkov, I. V. Kolbanev, L. G. Shcherbakova, *Solid State Ionics* **2005**, *176*, 2297.
[11] S. Nanamatsu, M. Kimura, *J. Phys. Soc. Jpn.* **1974**, *36*, 1495.
[12] S. Nanamatsu, M. Kimura, K. Doi, S. Matsushita, N. Yamada, *Ferroelectrics* **1974**, *8*, 511.
[13] V. V. Nemoshkalenko, S. V. Borisenko, V. N. Uvarov, A. N. Yaresko, A. G. Vakhney, A. I. Senkevich, T. N. Bondarenko, V. D. Borisenko, *Phys. Rev. B* **2001**, *63*, 075106.
[14] Y. Zhang, V. Shutthanandan, R. Devanathan, S. Thevuthasan, D. E. McCready, J. Young, G. Balakrishnan, D. M. Paul, W. J. Weber, *Nucl. Instrum. Methods Phys. Res. B* **2004**, *218*, 89.
[15] E. J. Harvey, K. R. Whittle, G. R. Lumpkin, R. I. Smith, S. A. T. Redfern, *J. Solid State Chem.* **2005**, *178*, 800.
[16] P. T. Diallo, P. B. Boutinaud, R. Mahiou, *J. Alloys Compd.* **2002**, *341*, 139.
[17] M. L. Pang, J. Lin, J. Fu, Z. Y. Cheng, M. L. Pang, *Mater. Res. Bull.* **2004**, *39*, 1607.
[18] H. H. Yang, H. Cheng, Y. G. Tang, Z. G. Lu, *J. Am. Ceram. Soc.* **2009**, *92*, 931.
[19] H. G. Kim, K. W. Hwang, S. W. Bae, J. H. Jung, J. S. Lee, *Catal. Lett.* **2003**, *91*, 193.
[20] F. X. Zhang, S. K. Saxena, *Chem. Phys. Lett.* **2005**, *413*, 248.
[21] Z. Li, G. Chen, X. Tian, Y. Li, *Mater. Res. Bull.* **2008**, *43*, 1781.
[22] H. B. Song, T. Y. Peng, P. Cai, H. B. Yi, C. H. Yan, *Catal. Lett.* **2007**, *113*, 54.
[23] Z. T. Zhao, Y. M. Zhang, J. Yang, H. Li, W. Song, X. Q. Zhao, *J. Ceram. Soc. Jpn.* **2005**, *113*, 67.
[24] D. S. Todorovsky, M. M. Getsova, M. A. Vasileva, *J. Mater. Sci.* **2002**, *37*, 4029.
[25] A. V. Prasadarao, U. Selvaraj, S. Komarneni, A. S. Bhalla, *J. Mater. Res.* **1992**, *7*, 2859.
[26] Z. Shao, S. Saitzek, P. Roussel, M. Huvé, R. Desfeux, O. Mentré, F. Abraham, *J. Cryst. Growth* **2009**, *311*, 4134.
[27] Z. Shao, S. Saitzek, P. Roussel, O. Mentré, F. P. Gheorghiu, L. Mitoseriu, R. Desfeux, *J. Solid State Chem.* **2010**, *183*, 1652.
[28] L. Vegard, *Z. Phys.* **1921**, *5*, 17.
[29] R. D. Shannon, *Acta Crystallogr., Sect. A* **1976**, *32*, 751.
[30] F. X. Zhang, B. Manoun, S. K. Saxena, C. S. Zha, *Appl. Phys. Lett.* **2005**, 86 181901.
[31] K. Krishnankutty, K. R. Dayas, *Bull. Mater. Sci.* **2008**, *31*, 907.
[32] L. J. Sham, M. Schlüter, *Phys. Rev. B* **1985**, *32*, 3883.
[33] E. Bruyer, A. Sayede, *J. Appl. Phys.* **2010**, *108*, 053705.
[34] D. W. Hwang, J. S. Lee, W. Li, S. H. Oh, *J. Phys. Chem. B* **2003**, *107*, 4963.
[35] R. Abe, M. Higashi, K. Sayama, Y. Abe, H. Sugihara, *J. Phys. Chem. B* **2006**, *110*, 2219.
[36] R. H. Abu-Eittah, S. A. Marie, M. B. Salem, *Can. J. Anal. Sci. Spectrosc.* **2004**, *49*, 248.
[37] L. K. Joseph, K. R. Dayas, S. Damodar, B. Krishnan, K. Krishnankutty, V. P. N. Nampoori, P. Radhakrishnan, *Spectrochim. Acta Part A* **2008**, *71*, 1281.
[38] G. H. Dieke, *Spectra and Energy Levels of Rare Earth Ions in Crystals*, Wiley-Interscience, New York, **1968**.
[39] G. Lakshminarayana, R. Yang, J. R. Qui, M. G. Brik, G. A. Kumar, I. V. Kityk, *J. Phys. D: Appl. Phys.* **2009**, *42*, 015414.
[40] L. Yang, X. Yu, S. Yang, C. Zhou, P. Zhou, W. Gao, P. Ye, *Mater. Lett.* **2008**, *62*, 907.
[41] C. K. Jayasankar, V. Venkatramu, P. Babu, Th. Tröster, W. Sievers, G. Wortmann, W. B. Holzapfel, *J. Appl. Phys.* **2005**, *97*, 093523.
[42] Y. C. Li, Y. H. Chang, Y. F. Lin, Y. S. Chang, Y. J. Lin, *J. Alloys Compd.* **2007**, *439*, 367.
[43] Y. Huang, W. kai, H. Lee, E. Cho, K. Jang, Y. Cao, W. Zhao, H. Ding, X. Wang, *Mater. Chem. Phys.* **2008**, *111*, 359.
[44] C. Qin, Y. Huang, W. Zhao, L. Shi, H. Seo, *Mater. Chem. Phys.* **2010**, *121*, 286.
[45] J. Trojan-Piegza, J. Niittykoski, J. Hölsä, E. Zych, *Chem. Mater.* **2008**, *20*, 2252.
[46] Y. Liu, J. Kuang, B. Lei, C. Shi, *J. Mater. Chem.* **2005**, *15*, 4025.
[47] B. Lei, Y. Liu, Z. Ye, C. Shi, *Mater. Chem. Phys.* **2004**, *87*, 227.
[48] G. Blasse, *Philips Res. Rep.* **1969**, *24*, 131.
[49] G. Blasse, *J. Solid State Chem.* **1986**, *62*, 207.
[50] Y. Tamura, A. Shibukawa, *Jpn. J. Appl. Phys.* **1993**, *32*, 3187.
[51] P. Blaha, K. Schwarz, G. K. H. Madsen,D. Kvasnicka, J. Luitz, Technische Universität Wien, Austria, **2002**.
[52] V. I. Anisimov, J. Zaanen, O. K. Andersen, *Phys. Rev. B* **1991**, *44*, 943.
[53] S. L. Dudarev, G. A. Botton, S. Y. Savrasov, C. J. Humphreys, A. P. Sutton, *Phys. Rev. B* **1998**, *57*, 1505.

Received: March 25, 2011
Published Online: July 15, 2011

